Biomacromolecules

pubs.acs.org/Biomac

Article

Solvent-Induced Assembly of Microbial Protein Nanowires into Superstructured Bundles

Yun-Lu Sun, Brian J. Montz, Ryan Selhorst, Hai-Yan Tang, Jiaxin Zhu, Kelly P. Nevin, Trevor L. Woodard, Alexander E. Ribbe, Thomas P. Russell, Stephen S. Nonnenmann,* Derek R. Lovley,* and Todd Emrick*

Cite This: *Biomacromolecules* 2021, 22, 1305−1311

Read Online

ACCESS | Metrics & More | Article Recommendations | Supporting Information

ABSTRACT: Protein-based electronic biomaterials represent an attractive alternative to traditional metallic and semiconductor materials due to their environmentally benign production and purification. However, major challenges hindering further development of these materials include (1) limitations associated with processing proteins in organic solvents and (2) difficulties in forming higher-order structures or scaffolds with multilength scale control. This paper addresses both challenges, resulting in the formation of one-dimensional bundles composed of electrically conductive protein nanowires harvested from the microbes *Geobacter sulfurreducens* and *Escherichia coli*. Processing these bionanowires from common organic solvents, such as hexane, cyclohexane, and DMF, enabled the production of multilength scale structures composed of distinctly visible pili. Transmission electron microscopy revealed striking images of bundled protein nanowires up to 10 μm in length and with widths ranging from 50−500 nm (representing assembly of tens to hundreds of nanowires). Conductive atomic force microscopy confirmed the presence of an appreciable nanowire conductivity in their bundled state. These results greatly expand the possibilities for fabricating a diverse array of protein nanowire-based electronic device architectures.

Superstructured Bundles of Conductive Protein Nanowires

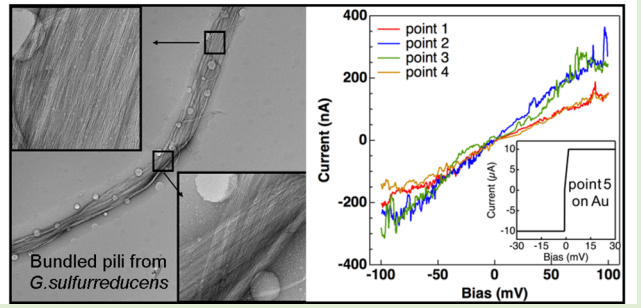

INTRODUCTION

A number of microorganisms express electrically conductive protein filaments that enable them to exchange electrons with other microbial species or minerals.[1−6] The protein nanowires of *Geobacter sulfurreducens*, assembled from PilA, a 61 amino acid protein composed primarily of an α-helix, have been studied extensively.[7,8] While the exact 3D structure of these pili has not been solved, they are hypothesized to consist of hexahelical assemblies of PilA that are associated via intramolecular forces (e.g., hydrogen bonding, $\pi-\pi$ stacking, and van der Waals attractions), which result in the microns long, 3 nm diameter filaments observed by atomic force microscopy (AFM) and transmission electron microscopy (TEM).[9] They are remarkably tolerant to conditions that often denature conventional proteins, such as elevated temperature and variable pH.[10−13] The detailed mechanism responsible for conductivity in *G. sulfurreducens* protein nanowires is not yet fully understood but appears to depend on the presence of aromatic amino acid residues.[7,8] Moreover, the conductivity of *G. sulfurreducens* protein nanowires has been tuned over a broad range (from 10^{-6} to 10^{3} S·cm^{-1}) via genetic alterations in the density of aromatic amino acids and pH modifications.[3,11,12,14] In the context of macromolecular bionanomaterials, protein nanowires open new opportunities to advance the field of sustainable electronics,[15,16] especially as methods are developed to process these structures into regular configurations amenable for integration into electronic material components.

Broadly considered, supramolecular protein assembly is a vibrant field with recent advances stemming from rational computational design and corresponding syntheses that project applications ranging from vaccine delivery to hydrogel formation to catalysis.[17−22] Mechanisms driving these protein assemblies include electrostatics, such as those responsible for fiber formation from velvet worms,[23] lock-and-key interactions in enzymes and lipid−antigen complexes,[24] and surface mediation, where roughness, topology, and charge influence the morphology of protein assembly into linear, fibrillar, or spherulitic structures.[25,26] High-resolution characterizations, including super resolution microscopy, total internal reflection fluorescence structured illumination microscopy (TIRF-SIM),

Received: December 21, 2020
Revised: January 12, 2021
Published: February 16, 2021

https://dx.doi.org/10.1021/acs.biomac.0c01790
Biomacromolecules 2021, 22, 1305−1311

and aberration-corrected cryogenic electron microscopy (cryo-EM), have been instrumental in advancing the precise characterization and visualization of these superstructures.[16,27] In addition to these synthetic constructs, naturally occurring types of supramolecular protein assemblies under investigation include amyloid fibrogens,[28] β-sheet assemblies,[17] ferritins,[29] and bacterial fibrils.[30]

Specifically considering protein nanowires composed of pilus-derived structures, prior reports have demonstrated their utility in devices when processed as films or mats, such as in the preparation of field-effect transistors.[10,31,32] In addition, prototype nanoscale device measurements have been performed on individual protein nanowires that are randomly deposited into a device configuration.[11,12] However, more rapid advancement of protein nanowire devices will require gaining morphological and dimensional control over the resultant superstructures. We note that aqueous suspensions of pili natively expressed by *E. coli* assemble into bundles and lattices in the presence of appropriate inducers.[33] However, the assembly of the relatively short (~1 μm), thick (diameter 6−7 nm), and electrically insulating *E. coli* pili cannot reliably guide studies of the longer, thinner, more flexible *G. sulfurreducens* protein nanowires.

This paper describes the use of organic solvents to process electrically conductive protein nanowires from *G. sulfurreducens* and a strain of *E. coli* expressing protein nanowires comprised of the *G. sulfurreducens* PilA monomer, where the solvent environment assists in driving nanowire assembly. We found that processing protein nanowires from common organic solvents induced the rapid production of quasi-2D bundles of nanowires. Electrical measurements performed on these bundles revealed an out-of-plane conductance approaching $\sim 10^{-6}$ S, confirming a retention of desirable electronic properties following this solvent processing. This fabrication approach is projected to create new opportunities to integrate protein nanowires into composite materials where organic solvent processing is advantageous or required for components of the composite material.

EXPERIMENTAL SECTION

Protein Nanowire Suspensions in Water. Protein nanowires were harvested from *Geobacter sulfurreducens* using physical shearing followed by multiple purification steps involving ammonium sulfate precipitation and resuspension in ethanolamine buffer.[3,31,34] Protein nanowires assembled in *E. coli* from the *G. sulfurreducens* PilA monomer were harvested by physical shearing, filtration, and resuspension in ethanolamine buffer.[35] For both sources of protein nanowires, the final product was dialyzed against water to remove buffer. The aqueous nanowire mixture (containing 0.1−0.6 μg/μL protein) was vortexed 5−6 times for 1−2 s at high power to resuspend the protein nanowires, and an aliquot was drop-cast onto the oxygen plasma-treated substrate (400 mesh, 3−4 nm carbon-coated copper TEM grids). Once deposited on the grid, the suspension was allowed to stand for 1 min, then wicked dry with filter paper, stained with 2 wt % aqueous uranyl acetate for 20−60 s, wicked dry a second time, and imaged using a JEOL 2000FX TEM at 200 kV accelerating voltage or a Tecnai T12 TEM at 120 kV.

Assembly of Protein Nanowires in Organic Solvents. *Method 1.* Protein nanowires were transferred from an aqueous suspension of *G. sulfurreducens* (48.5 μL aliquot containing 0.165 μg/μL protein) to a glass vial and dried under a stream of $N_{2(g)}$. An organic solvent (e.g., cyclohexane, hexane, or tetrahydrofuran) was added to a final concentration of 0.04−0.05 μg protein nanowires per μL. This mixture was vortexed 5−6 times for 1−2 s at high power and allowed to settle for ~10−30 min. The sample was then vortexed 1−2 times before transferring with a syringe to an oxygen plasma-treated substrate (400 mesh, 3−4 nm carbon-coated copper TEM grids or Si/SiO_2 wafers with gold electrodes) and drying in air. The TEM samples were stained for 1 min with 2 wt % aqueous uranyl acetate, wicked dry with filter paper, and imaged with a JEOL 2000FX TEM at 200 kV accelerating voltage.

Method 2. Protein nanowires (from genetically modified *E. coli*) were transferred from an aqueous suspension (30 μL aliquot containing 0.535 μg protein/μL) to a glass vial and dried under a stream of $N_{2(g)}$. An organic solvent (cyclohexane, hexane, THF, DMF, ACN, IPA, acetone, or *N*-methylformamide) was added to a final concentration of 0.10 μg nanowires per μL of solvent; the mixture was vortexed 5 times for ~1 second at high power and then allowed to settle for ~20 min. The samples were vortexed once before transferring 5 μL with a micropipette to an oxygen plasma-treated substrate (400 mesh, 3−4 nm carbon-coated copper TEM grids or Si/SiO_2 wafers with gold electrodes) and drying in air. The TEM samples were stained for 20 s with 4 μL of a 2 wt % aqueous uranyl acetate stain, wicked dry using filter paper, and imaged with an FEI Technai T-12 TEM at 120 kV accelerating voltage.

Assembly of Protein Nanowires in Mixed Aqueous-Organic Solvents. IPA (60 μL) was added to 20 μL of protein nanowires (~0.3 μg nanowire per μL) in ethanolamine buffer (150 mM, pH 10.5) and vortexed to resuspend the nanowires. The resultant suspension was allowed to settle for ~10−30 min and then was vortexed 1−2 times. This suspension (2−4 μL) was transferred to an oxygen plasma-treated substrate (400 mesh, 3−4 nm carbon-coated copper TEM grids or Si/SiO_2 wafer). Cyclohexane (20 μL) was added to the ethanolamine/IPA mixture, and the resulting mixture was vortexed 5−6 times for 1−2 s at high power. After allowing it to settle for ~10−30 min, the sample was vortexed 1−2 times before transferring with a syringe to an oxygen plasma-treated substrate (400 mesh, 3−4 nm carbon-coated copper TEM grids or Si/SiO_2 wafer) and drying in air. The TEM samples were stained with for 1 min with 2 wt % aqueous uranyl acetate, wicked dry using filter paper, and imaged with a JEOL 2000FX TEM at 200 kV accelerating voltage. Optical micrographs were obtained using an Olympus BX60 light microscope equipped with a Sony CCD-IRIS/RGB color video camera.

Hafnium Oxide Deposition. A 3 nm thick hafnia (HfO_2) film served as an insulating sample for c-AFM control experiments (this is similar in thickness to the diameter of the protein nanowires). These HfO_2 films were fabricated by atomic layer deposition (ALD, Cambridge Nanotech Savannah 100) at 250 °C for 45 cycles (0.67 Å/cycle) with a tetrakis(dimethylamido)hafnium ($Hf(NMe_2)_4$) precursor. The $Hf(NMe_2)_4$ and water ALD precursors were kept under separate conditions ($Hf(NMe_2)_4$ heated to 75 °C and H_2O at room temperature).

AFM Characterization. Conductive AFM (c-AFM) measurements were performed using a commercial system (Cypher ES, Asylum Research, Oxford Instrument; Goleta, CA) equipped with an ORCA dual-gain cantilever holder. Pt-coated conductive AFM tips (Nanoworld Arrow-CONTPt; Neuchâtel, Switzerland) were used for noncontact mode topographic imaging and for point-mode I-V spectroscopy in contact mode along the thickness direction of the protein nanowire bundles. The topography image was collected in noncontact mode under a scan rate of 1.0 Hz and setpoint of 0.02 V. Subsequently, the x-y piezo positioner translated the tip to the specific points on the bundle to perform point-mode *I*−*V* spectroscopy: the tip was first engaged onto a chosen point, and then, a bias between −100 and 100 mV, at a frequency of 0.2 Hz, was applied to the Au electrode. The currents across the bundle thickness to the tip (held at ground) were then recorded with the system using a transimpedance amplifier.

RESULTS AND DISCUSSION

Preparation and Characterization of Protein Nanowire Bundles. *G. sulfurreducens* is capable of producing three different types of nanowires: filaments homologous to type IV

https://dx.doi.org/10.1021/acs.biomac.0c01790
Biomacromolecules 2021, 22, 1305−1311

pili and comprised of the PilA monomer protein (3 nm diameter) and cytochrome-based wires comprised of the c-type cytochrome OmcS (4 nm diameter) or OmcZ (2.5 nm diameter).[7,34,36,37] For the experiments reported here, protein nanowires were grown and harvested using methods known to yield PilA-based protein nanowires (structurally depicted in Figure 1a) as confirmed by AFM analysis.[11,32,35] TEM

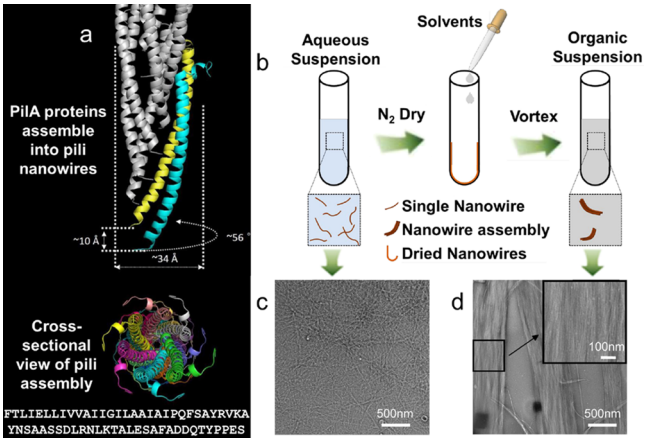

Figure 1. (a) 61 amino acid sequence of PilA (bottom) and a structural representation of a proposed assembly of PilA protein into pilus nanowires. Adapted from ref.,[38] copyright 2016, *Scientific Reports*; (b) schematic of the solvent exchange process in which protein nanowires are suspended initially in water and then in organic solvents; (c) TEM image of protein nanowires drop-cast from an aqueous suspension; (d) TEM image of protein nanowires that were resuspended in cyclohexane and then drop-cast onto a TEM grid, revealing pilus bundles (magnification shown in the upper right portion of the image).

characterization revealed that drop-casting a ~0.3 mg/mL aqueous dispersion of the nanowires onto an oxygen plasma-treated carbon-coated TEM grid produced a random nanowire network upon drying (Figure 1c). Similar random networks were obtained by drop-casting aqueous dispersions onto Si/SiO_2 wafers bridging gold electrodes.

In contrast to the results found with aqueous processing, the protein nanowires were seen to align into distinct bundles when aqueous nanowire suspensions were first dried under a stream of $N_{2(g)}$, then dispersed in an organic solvent (to a final concentration of ~0.05 mg/mL), and finally drop-cast onto the microscopy grid. For example, a cyclohexane dispersion of pili produced axially aligned, bundled superstructures that comprised distinct nanowire rows across their width, as shown in Figure 1d. Protein nanowires deposited from hexane dispersions produced long, extended, and twisted structures (Figure 2a; Figure S1). In some regions, hundreds of nanowires assembled side-by-side into flat ribbons (Figure 2a, left inset), while other regions appeared twisted. This ability of the bundles to fold over one other is featured in Figure 2a, and the more gradual bending observed in Figure 2b–d contributes to their flexibility. The solvent used in resuspension impacts the average lengths of the protein nanowire bundles (~2–5 μm), their average widths (~100–160 nm), and the average length of their linear segments (typically <2 μm). Both the flexibility and drapability of these superstructures are highlighted by the ~5.5 μm "loop" shown in Figure 2e. Protein nanowires deposited from THF showed splitting or multifurcation (Figure 2b), with multiple thinner

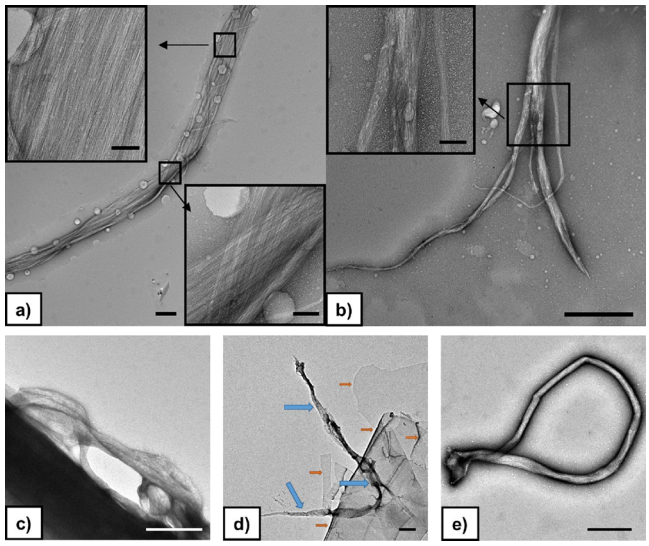

Figure 2. TEM images of *Geobacter* protein nanowire assemblies obtained from organic solvent dispersions in (a) hexane and (b) tetrahydrofuran. Scale bars: main images = 500 nm; insets = 100 nm; TEM images highlighting the flexibility of *E. coli* protein nanowire assemblies when drop-cast from organic solvents, using (c) cyclohexane, (d) DMF, and (e) IPA, for the dispersing media; scale bars: 500 nm. The circular features in (a) result from uranyl acetate staining. Blue arrows in (d) indicate the pilus bundles; red arrows highlight folds in the carbon film.

bundles emanating from the primary thicker structure. As shown in Figure 2 and Figure S2, processing from a broad selection of organic solvents leads to successful superstructure formation from the protein nanowires.

While the mechanism of this protein nanowire bundling is not fully understood, balancing the nonfavorable nanowire–solvent interactions in aprotic, apolar organic solvents clearly drives the interwire contact, seen in Figures 1 and 2. To investigate the effect of solvent composition on bundle morphology, the protein nanowires were suspended in polar aprotic solvents, including THF, acetone, DMF, and acetonitrile (ε = 7, 21, 37, 38, respectively), all of which successfully produced bundles; in contrast, pili cast from DMSO (ε = 47) appeared as individual, dispersed fibers. One polar protic solvent, isopropanol (IPA; ε = 18), led to bundled structures. Among these solvents, the lower dielectric constant examples led to superstructure formation, while the higher dielectric constant solvents tended toward nanowire dispersion in a similar fashion to the aqueous process (ε of H_2O ~80). Formamide, with a higher dielectric constant than water (ε ~110), also produced pilus dispersions, but surprisingly, the very high dielectric constant solvent *N*-methylformamide (NMF; ε ~180) produced pilus aggregates. This departure from the observed solvent trend is not understood but might be explained by the strong hydrogen bond donor and acceptor sites in NMF, which the literature suggests organizes the solvent into linear H-bonded chains.[39−41] Overall, while the organic solvent processing techniques we employed resulted in linear bundles with few branches, minor populations of branched and matlike structures are observed in some instances (Figure S8).

Interestingly, we find that protein nanowire bundling can also be achieved simply by pilus precipitation from mixed solvents without the need for the drying and redispersion

https://dx.doi.org/10.1021/acs.biomac.0c01790
Biomacromolecules 2021, 22, 1305−1311

protocol described above (Figure 3a). For example, Figure 3b–d shows TEM images of structures obtained by drop-

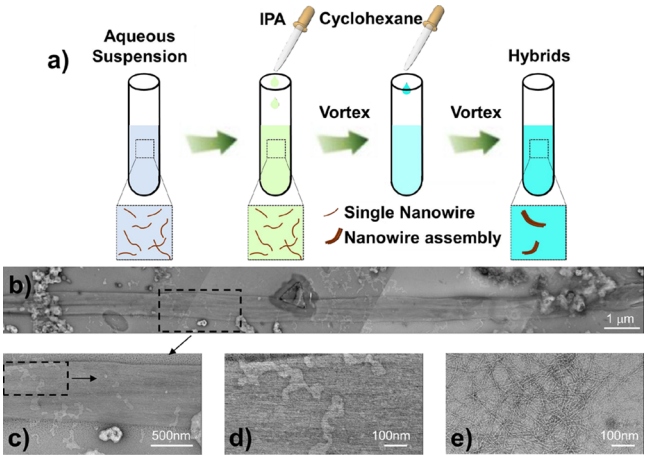

Figure 3. (a) Preparation of protein nanowire bundles from aqueous/organic solvent mixtures; (b–d) TEM images of the resultant bundles; (e) TEM image of dispersed protein nanowires obtained from ethanolamine/isopropanol mixtures (i.e., without cyclohexane addition).

casting a vortexed, slightly turbid dispersion of protein nanowires from a 1:3:1 miscible mixture (by volume) of ethanolamine buffer/isopropanol/cyclohexane. The macroscopic bundles revealed in these micrographs display similar features to those described above and are distinct from the appearance of the randomly oriented nanowires obtained from dispersions from 1:3 ethanolamine/isopropanol mixtures (Figure 3e). Use of aqueous/organic solvent mixtures also appear to increase the yield of protein nanowire bundles, following drop-casting of the nanowires from this solvent mixture onto a Si/SiO_2 wafer (Figure S3). Thus, the presence of cyclohexane promotes precipitation and bundling of the pili directly from a fluidic dispersion by reducing the favorability of pilus–solvent interactions in preference for pilus–pilus interactions.

We note that this observed dispersion and controlled bundling of protein nanowires processed in aqueous and organic media are distinct from the properties of more traditional nanomaterials, such as metallic nanowires and carbon nanotubes (CNTs). For example, CNTs agglomerate in aqueous solutions due to strong van der Waals attraction, thus requiring either organic dispersants that increase their electrical resistance[42] or ultrasonication that damages the nanotubes.[43,44] The protein nanowires studied here contrast these characteristics; in aqueous environments, they exhibit a randomized dispersion, while organic solvent processing induces agglomeration.

Local Current Response of Protein Nanowire Bundles. To determine whether the protein nanowires remained electrically conductive after assembly from organic solvents, electrical measurements were performed on samples that had been drop-cast from cyclohexane suspensions onto a Si/SiO_2 substrate with prepatterned Au microelectrodes. Noncontact AFM topographic imaging was employed to identify the location of protein nanowire bundles on the Au microelectrodes (Figure 4a and Figures S4A, S5A, S6A). The AFM setup used a bias applied through the bottom Au electrode and through the bundle, terminating at a grounded, Pt-coated

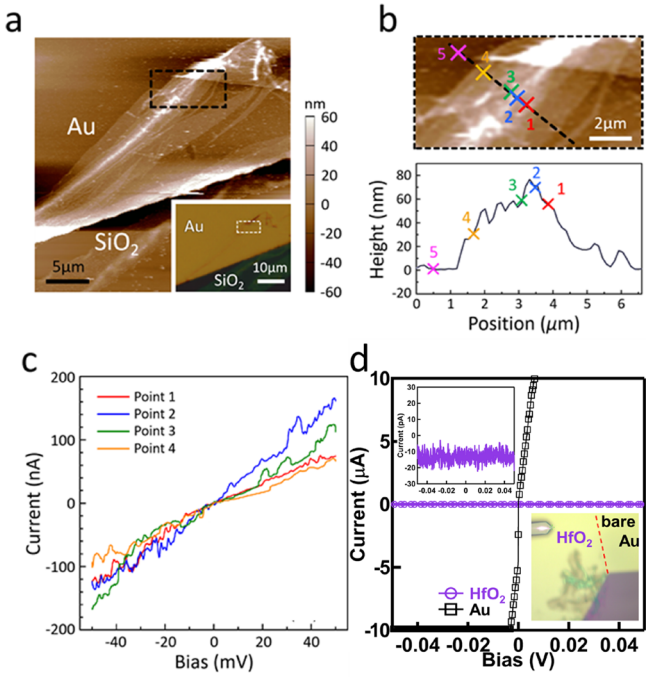

Figure 4. Conductive-AFM performed on a protein nanowire bundle drop cast from a protein/cyclohexane suspension on a gold surface. (a) Topographic image of a bundle (fold) on the gold surface. (b) Top: topographic image corresponding to the red rectangular area shown in (a) indicating the positions where data were recorded in the point-mode $I-V$ spectroscopy; bottom: cross-sectional height profile of the nanowire bundle across the red line shown in the top image; the x-symbols denote the locations where each $I-V$ curve was recorded; (c) Ohmic-like $I-V$ curves measured across the thickness of the bundle at points 1–4 shown in (b); (d) Au and HfO_2 c-AFM curves from direct Au electrode contact and through-thickness comparative measurements of a 3 nm ALD-deposited HfO_2 film. Upper inset: pA-level noise of the hafnia layer; lower inset: optical image of the AFM probe on the hafnia-covered Au microelectrode. Data on additional bundles are provided in Supplementary Figures S4–S6.

cantilever attached to a transimpedance amplifier to measure local current at multiple positions along transects across the bundles (Figure 4b and Figures S4B, S5B, S6B). The protein nanowire bundles exhibited Ohmic-like $I-V$ responses measured in the thickness direction for each of the contact points taken across the width (Figure 4c and Figures S4C, S5C, S6C). In contrast to the nA-level currents observed through the protein nanowire bundles, measurements taken directly on the Au electrode surface exceeded the 10 μA instrument protection threshold, even at a low applied bias (Figure 4c **inset**), and measurements taken on a 3 nm HfO_2 film, produced by ALD, registered pA-level noise, resulting in a through thickness current response at least 100 times lower than that of the least conductive protein nanowire bundle. The bundled superstructures exhibited conductance values, calculated from the linear slopes of the current–voltage curves, ranging from $1.4 \pm 0.5 \times 10^{-9}$ S to $2.3 \pm 0.5 \times 10^{-6}$ S. This broad conductance range would be expected from thickness-dependent variations in the current observed across the folded and bent areas observed in the inherently flexible bundles (Figure S7), though AFM tip contamination may also contribute to variations in response, where organic debris creates resistance within the circuit. While the noncontact

https://dx.doi.org/10.1021/acs.biomac.0c01790
Biomacromolecules 2021, 22, 1305–1311

topographic imaging employed here helps avoid contamination, future studies adopting point-mode fast-force mapping methods (typically used in nanomechanics)[45] to create fast current maps would further mitigate these issues by minimizing raster-based wear.

CONCLUSIONS

In summary, this study demonstrates that electrically conductive protein nanowires derived from *Geobacter sulfurreducens*, or produced by *E. coli* from the *G. sulfurreducens* pilin monomer PilA, assemble into bundles, comprised of sheetlike ribbons of nanowires, through processing with a wide range of common organic solvents, including hexane, THF, DMF, and IPA. These protein nanowire assemblies were visualized by TEM, exhibiting submicron widths (50−500 nm) of distinctly visible individual nanowires, lengths extending several microns (1.5−10 μm), and comprising of features markedly distinct from the random nanowire mats typically obtained from aqueous dispersion, where the majority of fibers were observed as individual filaments and occasional "bundles" were composed of 2−10 nanowires. cAFM through-thickness conductance measurements yielded out-of-plane conductance values as high as $2.3 \pm 0.5 \times 10^{-6}$ S, with a corresponding out-of-plane conductivity of ∼0.5 S/cm, confirming that the bundles retain desirable electrical properties following organic solvent processing. Similar currents are drawn by commercial microelectronic oscillators used in low speed internal/external clocks as well as ultra-low power accelerometers. The results suggest that conductive protein nanowires can be incorporated into composite materials that require organic solvent processing, with potential additional benefits of nanowire bundling for applications such as the fabrication of hybrid materials for stretchable electronics.

ASSOCIATED CONTENT

Supporting Information

The Supporting Information is available free of charge at https://pubs.acs.org/doi/10.1021/acs.biomac.0c01790.

TEM images of bundles from various solvents; optical micrograph of protein nanowires from the three-solvent system; c-AFM heightmap, cross-section profiles, and associated IV curves; and conductance *vs* bundle thickness plot (PDF)

AUTHOR INFORMATION

Corresponding Authors

Stephen S. Nonnenmann − *Department of Mechanical and Industrial Engineering, University of Massachusetts Amherst, Amherst, Massachusetts 01003, United States;* orcid.org/0000-0002-5369-9279; Email: ssn@umass.edu

Derek R. Lovley − *Department of Microbiology, University of Massachusetts Amherst, Amherst, Massachusetts 01003, United States;* orcid.org/0000-0001-7158-3555; Email: dlovley@microbio.umass.edu

Todd Emrick − *Department of Polymer Science and Engineering Department, University of Massachusetts Amherst, Amherst, Massachusetts 01003, United States;* orcid.org/0000-0003-0460-1797; Email: tsemrick@mail.pse.umass.edu

Authors

Yun-Lu Sun − *Department of Microbiology, University of Massachusetts Amherst, Amherst, Massachusetts 01003, United States*

Brian J. Montz − *Department of Polymer Science and Engineering Department, University of Massachusetts Amherst, Amherst, Massachusetts 01003, United States*

Ryan Selhorst − *Department of Polymer Science and Engineering Department, University of Massachusetts Amherst, Amherst, Massachusetts 01003, United States*

Hai-Yan Tang − *Department of Microbiology, University of Massachusetts Amherst, Amherst, Massachusetts 01003, United States*

Jiaxin Zhu − *Department of Mechanical and Industrial Engineering, University of Massachusetts Amherst, Amherst, Massachusetts 01003, United States*

Kelly P. Nevin − *Department of Microbiology, University of Massachusetts Amherst, Amherst, Massachusetts 01003, United States*

Trevor L. Woodard − *Department of Microbiology, University of Massachusetts Amherst, Amherst, Massachusetts 01003, United States*

Alexander E. Ribbe − *Department of Polymer Science and Engineering Department, University of Massachusetts Amherst, Amherst, Massachusetts 01003, United States*

Thomas P. Russell − *Department of Polymer Science and Engineering Department, University of Massachusetts Amherst, Amherst, Massachusetts 01003, United States;* orcid.org/0000-0001-6384-5826

Complete contact information is available at: https://pubs.acs.org/10.1021/acs.biomac.0c01790

Author Contributions

The manuscript and the work described within it involved contributions of all authors, and the authors have given approval to the final version of the manuscript.

Notes

The authors declare no competing financial interest.

ACKNOWLEDGMENTS

The authors acknowledge support for this work from the National Science Foundation (NSF-DMREF-1921839). The authors thank Max Zhang for performing ALD of the hafnia control sample and Jieun Park for performing c-AFM of the hafnia/Au control surfaces.

REFERENCES

(1) Reguera, G.; McCarthy, K. D.; Mehta, T.; Nicoll, J. S.; Tuominen, M. T.; Lovley, D. R. Extracellular Electron Transfer via Microbial Nanowires. *Nature* **2005**, *435*, 1098−1101.

(2) Summers, Z. M.; Fogarty, H. E.; Leang, C.; Franks, A. E.; Malvankar, N. S.; Lovley, D. R. Direct Exchange of Electrons Within Aggregates of an Evolved Syntrophic Coculture of Anaerobic Bacteria. *Science* **2010**, *330*, 1413−1415.

(3) Tan, Y.; Adhikari, R. Y.; Malvankar, N. S.; Ward, J. E.; Woodard, T. L.; Nevin, K. P.; Lovley, R. Expressing the Geobacter Metallireducens PilA in Geobacter Sulfurreducens Yields Pili with Exceptional Conductivity. *MBio* **2017**, *8*, 1−9.

(4) Walker, D. J.; Adhikari, R. Y.; Holmes, D. E.; Ward, J. E.; Woodard, T. L.; Nevin, K. P.; Lovley, D. R. Electrically Conductive Pili from Pilin Genes of Phylogenetically Diverse Microorganisms. *ISME J.* **2018**, *12*, 48−58.

(5) Walker, D. J. F.; Martz, E.; Holmes, D. E.; Zhou, Z.; Nonnenmann, S. S.; Lovley, D. R. The Archaellum of Methanospirillum Hungatei Is Electrically Conductive. *MBio* **2019**, *10*, 1−6.
(6) Walker, D. J. F.; Nevin, K. P.; Holmes, D. E.; Rotaru, A. E.; Ward, J. E.; Woodard, T. L.; Zhu, J.; Ueki, T.; Nonnenmann, S. S.; McInerney, M. J.; Lovley, D. R. Syntrophus Conductive Pili Demonstrate That Common Hydrogen-Donating Syntrophs Can Have a Direct Electron Transfer Option. *ISME J.* **2020**, *14*, 837−846.
(7) Lovley, D. R.; Walker, D. J. F. Geobacter Protein Nanowires. *Front. Microbiol.* **2019**, *10*, No. 2078.
(8) Lovley, D. R. Electrically Conductive Pili: Biological Function and Potential Applications in Electronics. *Curr. Opin. Electrochem.* **2017**, *4*, 190−198.
(9) Malvankar, N. S.; Vargas, M.; Nevin, K.; Tremblay, P. L.; Evans-Lutterodt, K.; Nykypanchuk, D.; Martz, E.; Tuomine, M. T.; Lovley, D. R. Structural Basis for Metallic-like Conductivity in Microbial Nanowires. *MBio* **2015**, *6*, 1−10.
(10) Malvankar, N. S.; Vargas, M.; Nevin, K. P.; Franks, A. E.; Leang, C.; Kim, B. C.; Inoue, K.; Mester, T.; Covalla, S. F.; Johnson, J. P.; Rotello, V. M.; Tuominen, M. T.; Lovley, D. R. Tunable Metallic-like Conductivity in Microbial Nanowire Networks. *Nat. Nanotechnol.* **2011**, *6*, 573−579.
(11) Adhikari, R. Y.; Malvankar, N. S.; Tuominen, M. T.; Lovley, D. R. Conductivity of Individual Geobacter Pili. *RSC Adv.* **2016**, *6*, 8354−8357.
(12) Tan, Y.; Adhikari, R. Y.; Malvankar, N. S.; Pi, S.; Ward, J. E.; Woodard, T. L.; Nevin, K. P.; Xia, Q.; Tuominen, M. T.; Lovley, D. R. Synthetic Biological Protein Nanowires with High Conductivity. *Small* **2016**, *12*, 4481−4485.
(13) Sun, Y. L.; Tang, H. Y.; Ribbe, A.; Duzhko, V.; Woodard, T. L.; Ward, J. E.; Bai, Y.; Nevin, K. P.; Nonnenmann, S. S.; Russell, T.; Emrick, T.; Lovley, D. R. Conductive Composite Materials Fabricated from Microbially Produced Protein Nanowires. *Small* **2018**, *14*, 1−5.
(14) Vargas, M.; Malvankar, N. S.; Tremblay, P. L.; Leang, C.; Smith, J. A.; Patel, P.; Synoeyenbos-West, O.; Nevin, K. P.; Lovley, D. R. Aromatic Amino Acids Required for Pili Conductivity and Long-Range Extracellular Electron Transport in Geobacter Sulfurreducens. *MBio* **2013**, *4*, 1−7.
(15) Lovley, D. R. E-Biologics : Fabrication of Sustainable Materials with "Green" Biological Materials. *MBio* **2017**, *8*, No. e00695.
(16) Kochovski, Z.; Chen, G.; Yuan, J.; Lu, Y. Cryo-Electron Microscopy for the Study of Self-Assembled Poly(Ionic Liquid) Nanoparticles and Protein Supramolecular Structures. *Colloid Polym. Sci.* **2020**, *298*, 707−717.
(17) Chen, C. H.; Hsu, E. L.; Stupp, S. I. Supramolecular Self-Assembling Peptides to Deliver Bone Morphogenetic Proteins for Skeletal Regeneration. *Bone* **2020**, *141*, No. 115565.
(18) Zottig, X.; Côté-Cyr, M.; Arpin, D.; Archambault, D.; Bourgault, S. Protein Supramolecular Structures: From Self-Assembly to Nanovaccine Design. *Nanomaterials* **2020**, *10*, 1−28.
(19) Dong, Y.; Mao, Y. DNA Origami as Scaffolds for Self-Assembly of Lipids and Proteins. *ChemBioChem* **2019**, *20*, 2422−2431.
(20) Ma, C.; Li, B.; Shao, B.; Wu, B.; Chen, D.; Su, J.; Zhang, H.; Liu, K. Anisotropic Protein Organofibers Encoded With Extraordinary Mechanical Behavior for Cellular Mechanobiology Applications. *Angew. Chem., Int. Ed.* **2020**, *59*, 21481−21487.
(21) Jain, R.; Pal, V. K.; Roy, S. Triggering Supramolecular Hydrogelation Using a Protein−Peptide Coassembly Approach. *Biomacromolecules* **2020**, *21*, 4180−4193.
(22) Ardini, M.; Huang, J. A.; Caprettini, V.; De Angelis, F.; Fata, F.; Silvestri, I.; Cimini, A.; Giansanti, F.; Angelucci, F.; Ippoliti, R. A Ring-Shaped Protein Clusters Gold Nanoparticles Acting as Molecular Scaffold for Plasmonic Surfaces. *Biochim. Biophys. Acta Gen. Subj.* **2020**, *1864*, No. 129617.
(23) Baer, A.; Hänsch, S.; Mayer, G.; Harrington, M. J.; Schmidt, S. Reversible Supramolecular Assembly of Velvet Worm Adhesive Fibers via Electrostatic Interactions of Charged Phosphoproteins. *Biomacromolecules* **2018**, *19*, 4034−4043.
(24) Borg, N. A.; Wun, K. S.; Kjer-Nielsen, L.; Wilce, M. C. J.; Pellicci, D. G.; Koh, R.; Besra, G. S.; Bharadwaj, M.; Godfrey, D. I.; McCluskey, J.; Rossjohn, J. CD1d-Lipid-Antigen Recognition by the Semi-Invariant NKT T-Cell Receptor. *Nature* **2007**, *448*, 44−49.
(25) Yang, B.; Adams, D. J.; Marlow, M.; Zelzer, M. Surface-Mediated Supramolecular Self-Assembly of Protein, Peptide, and Nucleoside Derivatives: From Surface Design to the Underlying Mechanism and Tailored Functions. *Langmuir* **2018**, *34*, 15109−15125.
(26) Yagi, H.; Ban, T.; Morigaki, K.; Naiki, H.; Goto, Y. Visualization and Classification of Amyloid β Supramolecular Assemblies. *Biochemistry* **2007**, *46*, 15009−15017.
(27) Simpson, L. W.; Good, T. A.; Leach, J. B. Protein Folding and Assembly in Confined Environments: Implications for Protein Aggregation in Hydrogels and Tissues. *Biotechnol. Adv.* **2020**, *42*, No. 107573.
(28) Ghahghaei, A.; Faridi, N. Review: Structure of Amyloid Fibril in Diseases. *J. Biomed. Sci. Eng.* **2009**, *02*, 345−358.
(29) Uchida, M.; Kang, S.; Reichhardt, C.; Harlen, K.; Douglas, T. The Ferritin Superfamily: Supramolecular Templates for Materials Synthesis. *Biochim. Biophys. Acta Gen. Subj.* **2010**, *1800*, 834−845.
(30) Hainline, K. M.; Fries, C. N.; Collier, J. H. Progress Toward the Clinical Translation of Bioinspired Peptide and Protein Assemblies. *Adv. Healthcare Mater.* **2018**, *7*, 1−12.
(31) Liu, X.; Gao, H.; Ward, J. E.; Liu, X.; Yin, B.; Fu, T.; Chen, J.; Lovley, D. R.; Yao, J. Power Generation from Ambient Humidity Using Protein Nanowires. *Nature* **2020**, *578*, 550−554.
(32) Smith, A. F.; Liu, X.; Woodard, T. L.; Fu, T.; Emrick, T.; Jiménez, J. M.; Lovley, D. R.; Yao, J. Bioelectronic Protein Nanowire Sensors for Ammonia Detection. *Nano Res.* **2020**, *13*, 1479−1484.
(33) Cao, B.; Xu, H.; Mao, C. Controlled Self-Assembly of Rodlike Bacterial Pili Particles into Ordered Lattices. *Angew. Chem., Int. Ed.* **2011**, *50*, 6264−6268.
(34) Filman, D. J.; Marino, S. F.; Ward, J. E.; Yang, L.; Mester, Z.; Bullitt, E.; Lovley, D. R.; Strauss, M. Cryo-EM Reveals the Structural Basis of Long-Range Electron Transport in a Cytochrome-Based Bacterial Nanowire. *Commun. Biol.* **2019**, *2*, 19−24.
(35) Ueki, T.; Walker, D. J. F.; Woodard, T. L.; Nevin, K. P.; Nonnenmann, S. S.; Lovley, D. R. An Escherichia Coli Chassis for Production of Electrically Conductive Protein Nanowires. *ACS Synth. Biol.* **2020**, *9*, 647−654.
(36) Yalcin, S. E.; O'Brien, J. P.; Gu, Y.; Reiss, K.; Yi, S. M.; Jain, R.; Srikanth, V.; Dahl, P. J.; Huynh, W.; Vu, D.; Acharya, A.; Chaudhuri, S.; Varga, T.; Batista, V. S.; Malvankar, N. S. Electric Field Stimulates Production of Highly Conductive Microbial OmcZ Nanowires. *Nat. Chem. Biol.* **2020**, *16*, 1136−1142.
(37) Wang, F.; Gu, Y.; O'Brien, J. P.; Yi, S. M.; Yalcin, S. E.; Srikanth, V.; Shen, C.; Vu, D.; Ing, N. L.; Hochbaum, A. I.; Egelman, E. H.; Malvankar, N. S. Structure of Microbial Nanowires Reveals Stacked Hemes That Transport Electrons over Micrometers. *Cell* **2019**, *177*, 361−369.e10.
(38) Xiao, K.; Malvankar, N. S.; Shu, C.; Martz, E.; Lovley, D. R.; Sun, X. Low Energy Atomic Models Suggesting a Pilus Structure That Could Account for Electrical Conductivity of Geobacter Sulfurreducens Pili. *Sci. Rep.* **2016**, *6*, 1−9.
(39) Bass, S. J.; Nathan, W. I.; Meighan, R. M.; Cole, R. H. Dielectric Properties of Alkyl Amides. II. Liquid Dielectric Constant and Loss. *J. Phys. Chem.* **1964**, *68*, 509−515.
(40) Richardi, J.; Krienke, H.; Fries, P. H. Dielectric Constants of Liquid Formamide, N-Methylformamide and Dimethylformamide via Molecular Ornstein-Zernike Theory. *Chem. Phys. Lett.* **1997**, *273*, 115−121.
(41) Barthel, J.; Buchner, R.; Wurm, B. The Dynamics of Liquid Formamide, N-Methylformamide, N,N-Dimethylformamide, and N,N-Dimethylacetamide. A Dielectric Relaxation Study. *New York* **2002**, *98-99*, 51−69.
(42) Hobbie, E. K.; Obrzut, J.; Kharchenko, S. B.; Grulke, E. A. Charge Transport in Melt-Dispersed Carbon Nanotubes. *J. Chem. Phys.* **2006**, *125*, 1−4.

https://dx.doi.org/10.1021/acs.biomac.0c01790
Biomacromolecules 2021, 22, 1305−1311

(43) Mutiso, R. M.; Sherrott, M. C.; Li, J.; Winey, K. I. Simulations and Generalized Model of the Effect of Filler Size Dispersity on Electrical Percolation in Rod Networks. *Phys. Rev. B - Condens. Matter Mater. Phys.* **2012**, *86*, 1−6.
(44) Moniruzzaman, M.; Winey, K. I. Polymer Nanocomposites Containing Carbon Nanotubes. *Macromolecules* **2006**, *39*, 5194−5205.
(45) Kocun, M.; Labuda, A.; Meinhold, W.; Revenko, I.; Proksch, R. Fast, High Resolution, and Wide Modulus Range Nanomechanical Mapping with Bimodal Tapping Mode. *ACS Nano* **2017**, *11*, 10097−10105.

https://dx.doi.org/10.1021/acs.biomac.0c01790
Biomacromolecules 2021, 22, 1305−1311